Covalent Binding of Biological Samples to Solid Supports for Scanning Probe Microscopy in Buffer Solution

Simone Karrasch,* Max Dolder,* Frank Schabert,* Jeremy Ramsden,‡ and Andreas Engel*
*Maurice E. Müller-Institute for High-Resolution Electron Microscopy and ‡Department of Biophysical Chemistry at the Biocenter of the University of Basel, Basel, Switzerland

ABSTRACT Scanning force microscopy allows imaging of biological molecules in their native state in buffer solution. To this end samples have to be fixed to a flat solid support so that they cannot be displaced by the scanning tip. Here we describe a method to achieve the covalent binding of biological samples to glass surfaces. Coverslips were chemically modified with the photoactivatable cross-linker *N*-5-azido-2-nitrobenzoyloxysuccinimide. Samples are squeezed between derivatized coverslips and then cross-linked to the glass surface by irradiation with ultraviolet light. Such samples can be imaged repeatedly by the scanning force microscope without loss of image quality, whereas identical but not immobilized samples are pushed away by the stylus.

INTRODUCTION

The scanning force microscope (SFM) (Binnig et al., 1986) has allowed imaging of many organic and inorganic materials up to atomic scale resolution (Albrecht and Quate, 1987; Binnig et al., 1987; Manne et al., 1991; Alves et al., 1992; Hillner et al., 1992), but so far this has not been achieved with biological macromolecules. Molecular resolution has been demonstrated by images of purple membranes (Butt et al., 1990), gap junctions (Hoh et al., 1993), and fibrinogen molecules (Drake et al., 1989), all recorded in buffer solution. Imaging in solution requires the samples to be fixed to a suitable support so that they cannot be displaced by the scanning tip. Some membranes and other supramolecular assemblies adhere strongly to freshly cleaved mica in the presence of the appropriate counterions (Butt et al., 1990; Hoh et al., 1993). Plasmid-DNA and DNA-protein complexes could be imaged in propanol by using mica treated with magnesium acetate (Hansma et al., 1992; Vesenka et al., 1992b; Shaiu et al., 1993). Alternatively, various substrates have been reacted with 3-aminopropyltriethoxysilane (APTES) and methylated to generate quarternary amines to which DNA could be bound efficiently to be imaged in air, propanol, and water (Lyubchenko et al., 1993). In addition, APTES-treated glass has been used as a substrate for purple membranes (Butt et al., 1990). These methods take advantage of electrostatic interactions between the sample, the support, and different ions and work best for large charged or polar structures. Immobilization of uncharged biomacromolecules on a flat solid support requires alternative methods.

Immobilization of proteins is important for a number of different applications (Robinson et al., 1971; Wachter et al., 1973; Quash et al., 1978; Hendry and Rauch, 1980; Aebersold et al., 1986; Brode and Rauch, 1992). Thus, binding of proteins to charged surfaces like polylysine-coated beads (Jacobson and Branton, 1977) and methods for covalent binding to other substrates have been developed (Weetall, 1976). The substrates used include glass beads (Wachter et al., 1973), glass filter paper (Aebersold et al., 1986), polystyrene (Machleidt and Wachter, 1977), and latex particles (Quash et al., 1978), as well as flat solid supports suitable for scanning probe microscopy such as silicon wafers, mica (Lyubchenko et al., 1993), and glass slides (Aplin et al., 1981).

Here we present a simple and reproducible protocol to cross-link biological samples to a chemically modified glass surface. Conditions to derivatize a clean glass surface with APTES and to react the amino groups with the photoactivatable cross-linker *N*-5-azido-2-nitrobenzoyloxysuccinimide (ANB-NOS) are described. Different supramolecular structures were covalently immobilized to such modified glass surfaces and imaged in buffer solution by scanning force microscopy at high resolution.

MATERIALS AND METHODS

Materials

Round glass coverslips with a diameter of 1 cm were from Plano (W. Plannet GmbH, Marburg, Germany). APTES, *N*-5-azido-2-nitrobenzoic acid, *p*-azidophenylisothiocyanate, dimethylformamid, dicyclohexylcarbodiimide, tetrahydrofuran, trifluoroacetic acid, and chemicals for the ninhydrin reaction were purchased from Fluka Chemie AG (Buchs, Switzerland). Sulfosuccinimidyl 2-(*m*-azido-*o*-nitrobenzamido)-ethyl-1,3′-dithiopropionate, bis(sulfosuccinimidyl) suberate and *N*-hydroxysuccinimide were from Pierce (Rockford, IL). ANB-NOS was synthesized as described by Lewis et al. (1977). Disuccinimidyl tartrate and disulfosuccinimidyl tartrate were synthesized as described by Smith et al. (1978) and Anderson et al. (1964). Poly-L-lysine and alkaline phosphatase type III from *Escherichia coli* were from Sigma Chemical Co. (St. Louis, MO). All other chemicals were from E. Merck (Darmstadt, Germany).

A-type polyheads were prepared as described by Steven et al. (1976) using a 20^- mutant of T4 bacteriophages. The mutants were propagated and titrated on the permissive host *E. coli* CR 63. *E. coli* B^e was used as the nonpermissive host for the production of polyheads.

Received for publication 11 June 1993 and in revised form September 9, 1993.

Address reprint requests to Dr. Engel, M. E. Müller-Institute, Biocenter, University of Basel, Klingelbergstrasse 70, CH-4056 Basel, Switzerland.

0006-3495/93/12/2437/10 $2.00

The hexagonally packed intermediate layer (HPI layer) of *Deinococcus radiodurans* was a gift of Dr. Wolfgang Baumeister (Max-Planck-Institute for Biochemistry, Martinsried).

Intermediate filaments were assembled in vitro from recombinant neurofilament protein NF-L expressed in *E. coli* (Heins et al., 1993).

Tobacco mosaic virus (TMV) was a gift of Dr. Jean Witz, Institut de Biologie Moleculaire et Cellulaire, Strasbourg, France.

Modification of glass surfaces

Silanization and derivatization of coverslips were carried out in Petri dishes that had been washed in "piranha bath" (3.5% H_2O_2 in 18 M H_2SO_4), followed by rinsing with water and acetone. The following steps were carried out at room temperature unless stated otherwise. Coverslips were washed once with concentrated HCl/HNO_3 (3:1) and five times for 1 min with distilled water in an ultrasonic bath (50 kHz). They were etched with trifluoroacetic acid for 90 min and stored in vacuum over solid KOH for at least 10 h. Coverslips were then silanized with APTES (2% in 95% aqueous acetone) for 3 min followed by washing with acetone (12 times, 5 min each) according to Aebersold et al. (1986). Curing of the silane linkages was carried out in an oven at 110°C for 1 h. All subsequent steps were performed in the darkroom using red safety light. The reaction of the NH_2 groups with the succinimide ester group of ANB-NOS was carried out in 0.1 M Na_2CO_3, pH 9.0. The reaction mixture was prepared by adding 10 nmol ANB-NOS/cm^2 glass surface dissolved in 1 ml dioxane to 20 ml Na_2CO_3 solution. This corresponds to a 10-fold molar excess of the photocross-linker with respect to the amino groups. The coverslips were incubated for 4 h. Excess reagent was then removed by washing the coverslips three times with 1% butylamine in 0.1 M Na_2CO_3, three times with 0.1 M Na_2CO_3, two times with distilled water, and two times with acetone. Coverslips were stored under vacuum and handled in the dark.

For the covalent binding of samples to the modified glass surface, the coverslips were squeezed between two glass disks (borosilicate safety sight glass; diameter = 12 cm, thickness = 2 cm) at a pressure of 100 to 5×10^3 N/cm^2 to bring the hydrophilic biological structures into close contact with the hydrophobic cross-linker. Covalent coupling of the samples was induced by activating the azide with ultraviolet (UV) irradiation at 366 nm (Sylvania F8T5) at a distance of 10 cm for 3 min. The extent of the reaction was determined from the change in the absorption band of ANB-NOS at 312 nm (Fig. 1). Coverslips were rinsed thoroughly with water to remove excess protein and stored in water or buffer. To illustrate that the reaction of the photogenerated nitrene with the protein is the most important step for immobilizing the samples, derivatized coverslips were also exposed to UV light before sample deposition and examination by the SFM.

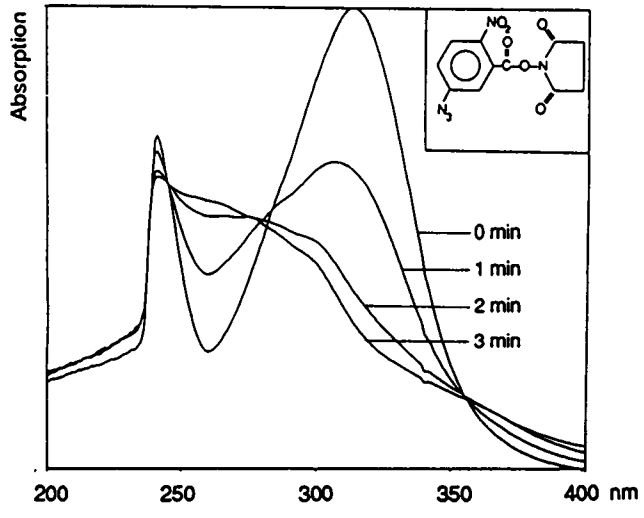

FIGURE 1 UV spectrum of the photoreactive cross-linker ANB-NOS (in chloroform) after irradiation at 366 nm for 0, 1, 2, and 3 min. The absorption maximum at 312 nm results from the azido group, and its decrease corresponds to the activation of the azide. The two reactive groups of ANB-NOS are the succinimide ester and the photoactivatable azide (*inset*).

Immobilization with polylysine

Acid-washed coverslips were coated with a polylysine solution (10 mg/ml; M_r 1000–4000), washed with water after 1 min and dried in air. The protein solution (3 mg/ml) was deposited on the dry surface and washed off after 15 min. Adsorbed structures were then examined in the SFM.

Scanning electron microscopy (SEM)

The samples were air-dried and coated with Pt/C. SEM was performed on a Hitachi S-800 scanning electron microscope operated at 30 kV.

Analytical procedures

1. The number of NH_2 groups per glass surface area after silanization was measured with ninhydrin as described by Sarin et al. (1981).

2. To determine the amount of protein that can be coupled to the derivatized glass surfaces, 2 μl alkaline phosphatase (7 mg/ml) were deposited on the coverslips and immobilized using the protocol above. The enzyme activity was then assayed as described in the Worthington Enzyme Manual (Decker, 1977) using *p*-nitrophenyl phosphate as substrate. Calibration plots were made with different enzyme dilutions. The enzyme concentration on the coverslips was determined from the measured enzyme activity and the known specific activity of alkaline phosphatase (AP).

3. The hydrophobicity of the glass surfaces after the different treatments was assessed by measuring the diameter of 10-μl water droplets deposited on the coverslips (Engel et al., 1992).

4. To obtain a quantitative measure of the substrate surface roughness, 30–40 images of 10-μm sidelength were recorded from substrates after each processing step, a plane-fit carried out and the root-mean-square deviation of the *z* values calculated, all taking advantage of the software provided by Digital Instruments (Santa Barbara, CA). In addition, one typical image from each step was transferred to the SEMPER image processing system (Synoptics Ltd., Cambridge, England) (Saxton et al., 1979) to analyze the particle density and size distribution. The particle size was calculated from the particle areas assuming circular shape.

Instrumentation

A Nanoscope III scanning force microscope (Digital Instruments) equipped with a scanning tube for scan widths of 125 μm was used. The coverslips were dried on the backside, glued on steel disks, and mounted at the top of the scanner. Cantilevers from Digital with a spring constant k = 0.38 N/m and a pyramid-shaped tip were used (Albrecht et al., 1990). In some cases they were provided with sharp carbon protrusions deposited with the electron beam of a Hitachi S-800 scanning electron microscope (Keller and Chin-Chung, 1992). All SFM measurements were performed at ambient pressure, room temperature, and in phosphate buffer (100 mM potassium phosphate, pH 7.0, 1 mM $MgSO_4$). The scan speed varied between 1 and 600 nm/s, depending on the scan size. The forces were approximately 1 nN as determined from force curves (Weisenhorn et al., 1989).

RESULTS

Characterization of chemically modified coverslips

As outlined in Fig. 2, glass surfaces coated with cross-linker molecules are obtained by a two-step procedure: (i) silanization with APTES (Fig. 2 *a*) and (ii) derivatization with the

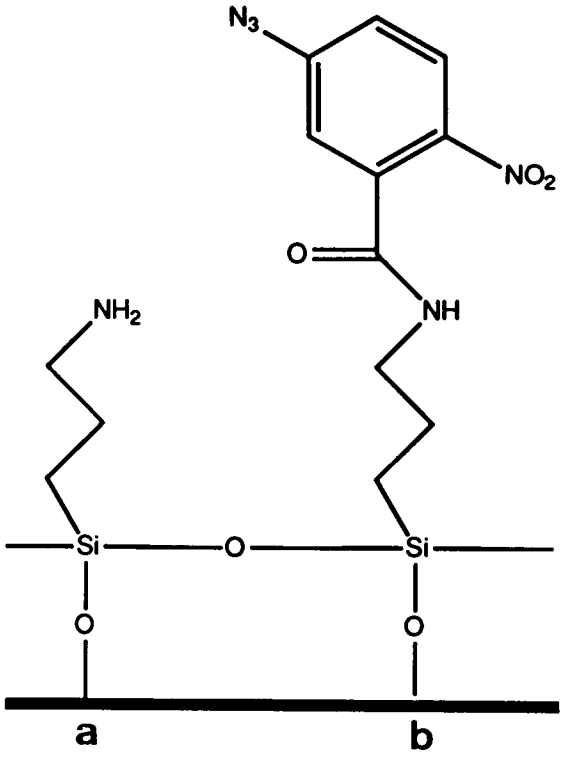

FIGURE 2 Schematic diagrams of the glass surface after (*a*) silanization with APTES and (*b*) derivatization with the photoreactive cross-linker ANB-NOS.

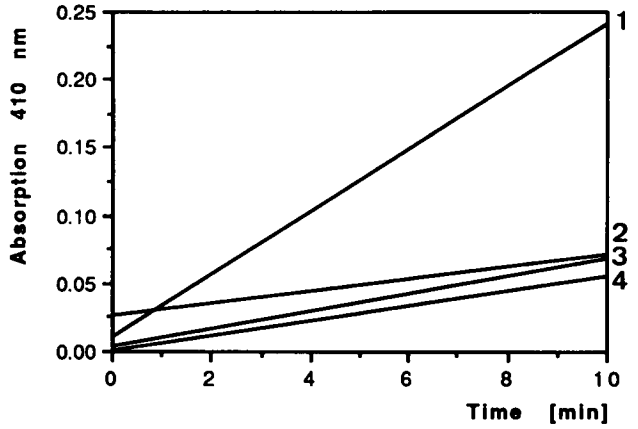

FIGURE 3 Activity of alkaline phosphatase monitored by absorbance at 410 nm on (*1*) derivatized, (*2*) silanized, (*3*) derivatized/preirradiated, and (*4*) untreated coverslips.

photoreactive cross-linker ANB-NOS (Fig. 2 *b*). The silanization protocol resulted in approximately 1 nmol NH_2 groups/cm^2 glass surface as determined with the ninhydrin reaction, which corresponds to an average of 6 NH_2 groups/nm^2. To ensure a surface tightly packed with photoreactive groups, ANB-NOS was applied in a 10-fold molar excess over the amino groups. AP was used to estimate the amount of protein that can be coupled to the glass surface by the cross-linker. The enzyme exhibited a turnover rate of 5 nmol *p*-nitrophenol/(min × cm^2 glass surface). UV irradiation and addition of soluble ANB-NOS did not influence the activity of AP as determined with control experiments (data not shown). Therefore, the measured turnover rate corresponds to 0.01 nmol immobilized AP/cm^2 as determined from calibration plots, i.e., 17 nm^2 per AP molecule, indicating a tight packing on the coverslips. In contrast, AP deposited on untreated, silanized, or derivatized/preirradiated coverslips exhibits only ~20% of the measured turnover rate of AP coupled to derivatized coverslips (Fig. 3). This residual activity is presumably due to unspecific binding of AP molecules to the glass surface.

The surface roughness of the glass was monitored throughout the procedure (Fig. 4). A quantitative comparison was achieved by recording 30–35 images of 10 μm sidelength after each modification step, calculating the root-mean-square deviation of the *z*-values, and analyzing the particle density and size distribution (see "Materials and Methods"). The washing step with acid in the ultrasonic bath is efficient for eliminating dust, organic contaminants, and other particles (Fig. 4 *a*). The result of this procedure is a smooth, clean surface exhibiting a mottled background and less than 1 particle/μm^2 (Fig. 4 *b*, Table 1). After silanization the surface roughness increases as a result of increased particle density (Fig. 4 *c*, Table 1). The particle density is further increased by derivatization, and a distinct enlargement of the particles is apparent (Fig. 4 *d*, Table 1). The surface texture of the modified coverslips can be discriminated from the biological samples used in this work. The hydrophobicity of the coverslips after the different treatments was assessed by examining water droplets of a fixed volume deposited on the glass surface (Engel et al., 1992). As indicated in Table 2, their diameter is a sensitive indicator of hydrophobicity: while the surfaces of washed and etched coverslips are hydrophilic, the coverslips are more hydrophobic after silanization and derivatization.

Immobilization and imaging of biological structures in buffer solution

Biomacromolecules and supramolecular assemblies had to be in close proximity with the photogenerated nitrene to become immobilized. To achieve this, high protein concentrations (1–10 mg/ml) and clamping of the coverslips between UV translucent glass plates were used. As illustrated with the following examples, a variety of proteins could be covalently bound to the derivatized glass surface.

Bacteriophage T4 polyheads

Polyheads are tubular structures folded from a hexagonal lattice ($a = b = 13$ nm) of capsomeres, each containing six major T-even bacteriophage head polypeptides (gp 23) (Steven et al., 1976). These tubes have a diameter of 50–65 nm and vary in length (up to several micrometers). Upon drying in air or adsorption to a glow-discharged carbon film, the tubes collapse into planar double layers. After cross-linking to derivatized glass surfaces the polyheads can be

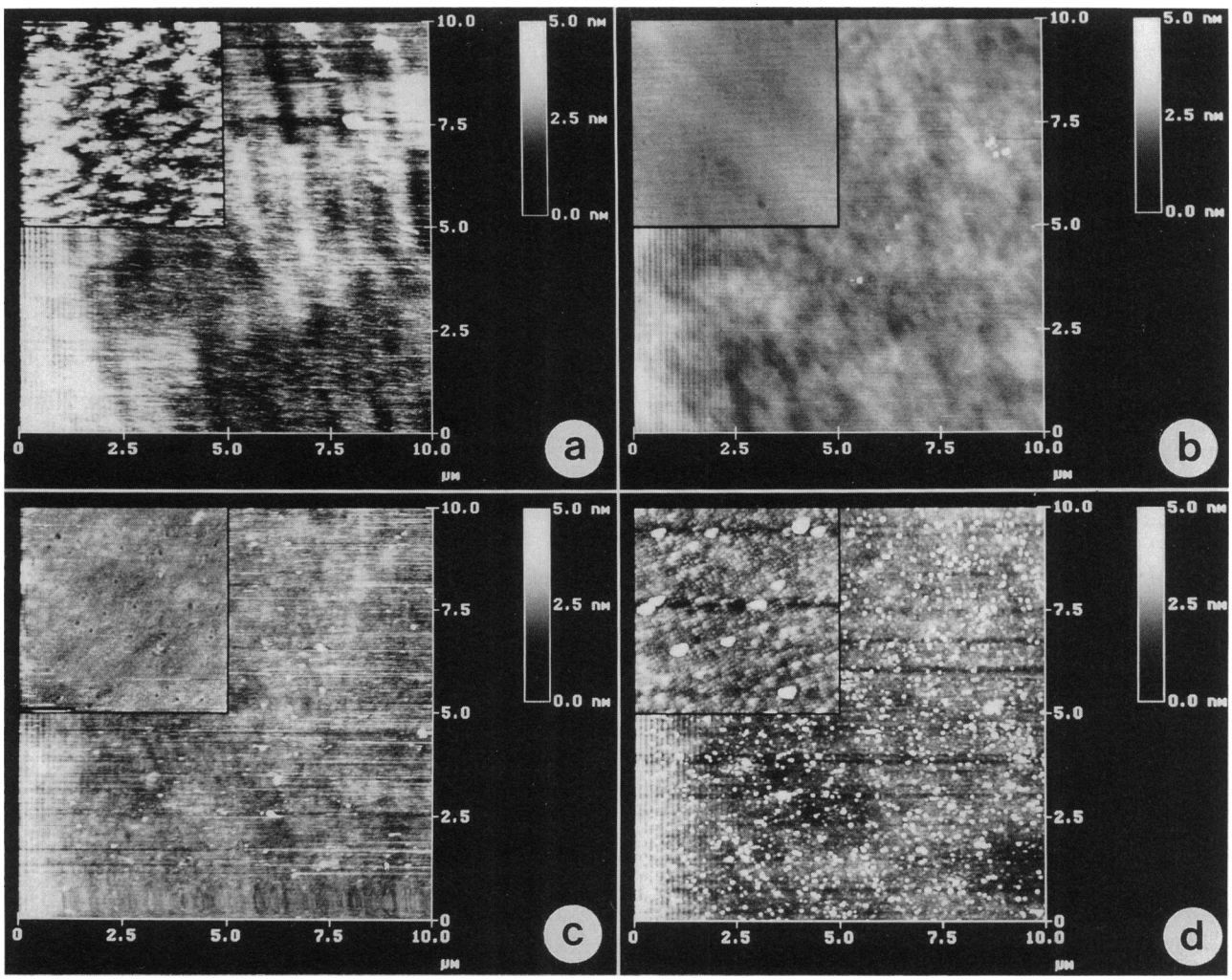

FIGURE 4 Surface roughness during the modification of the coverslips as assessed by SFM images: (*a*) untreated (= without any washing, just taken out of the box), (*b*) acid washed, (*c*) silanized, and (*d*) derivatized glass surfaces. Insets are 1 × 1 μm.

TABLE 1 Surface roughness analysis of glass substrates after different chemical modifications

Modification	RMS (nm)	Particles/μm²	Particle size (nm)
Untreated	1.50 ± 1.07		
Acid-washed	0.45 ± 0.08	0.3 ± 0.2	46 (33, 144)
Silanized	1.02 ± 0.37	0.7 ± 0.3	37 (24, 112)
Derivatized	1.54 ± 0.24	5.7 ± 1.4	38 (20, 200)
Silicon wafer, acid-washed	0.45 ± 0.07	0.9 ± 0.1	40 (22, 58)

The root-mean-square (RMS) deviations of *z* values were calculated with the software provided by Digital Instruments. The number of particles per area, their median size, and the minimum and maximum sizes given in parentheses were evaluated with the SEMPER image processing system. Frames of 10-μm sidelength with a pixel size of 20 nm were analyzed (Fig. 4).

TABLE 2 Diameter of 10-μl water droplets deposited on the glass surface after different modifications

Modification	Diameter (mm)
Washed	7.4 ± 0.7 (n=50)
Etched	7.5 ± 0.7 (n=50)
Silanized	4.1 ± 0.2 (n=40)
Derivatized	4.7 ± 0.2 (n=40)
Silanized and incubated at pH 10 for 4 h	4.3 ± 0.1 (n=30)

repeatedly imaged at low (Fig. 5 *a*) and high (Fig. 5 *b*) magnification by SFM. The majority of background particles are viral structures as revealed by electron micrographs of a negatively stained control. As demonstrated by these images, the polyheads retained a cylindrical cross-section during preparation and imaging in phosphate buffer. Their width and height were 151 ± 30.9 nm (n = 30) and 57 ± 13.8 nm (n = 30), respectively. The capsomeres are well resolved and exhibit the characteristic pattern of gp 23 hexamers. They are particularly clear at the top of the cylinder, whereas they appear distorted at the periphery as a result of their tilt with respect to the stylus. While a control preparation of polyheads adsorbed to preirradiated/derivatized coverslips was also densely covered, stable imaging conditions could not be established. A single scan at medium magnification (Fig. 5 *c*) was sufficient to wipe the surface clean (Fig. 5 *d*). Under

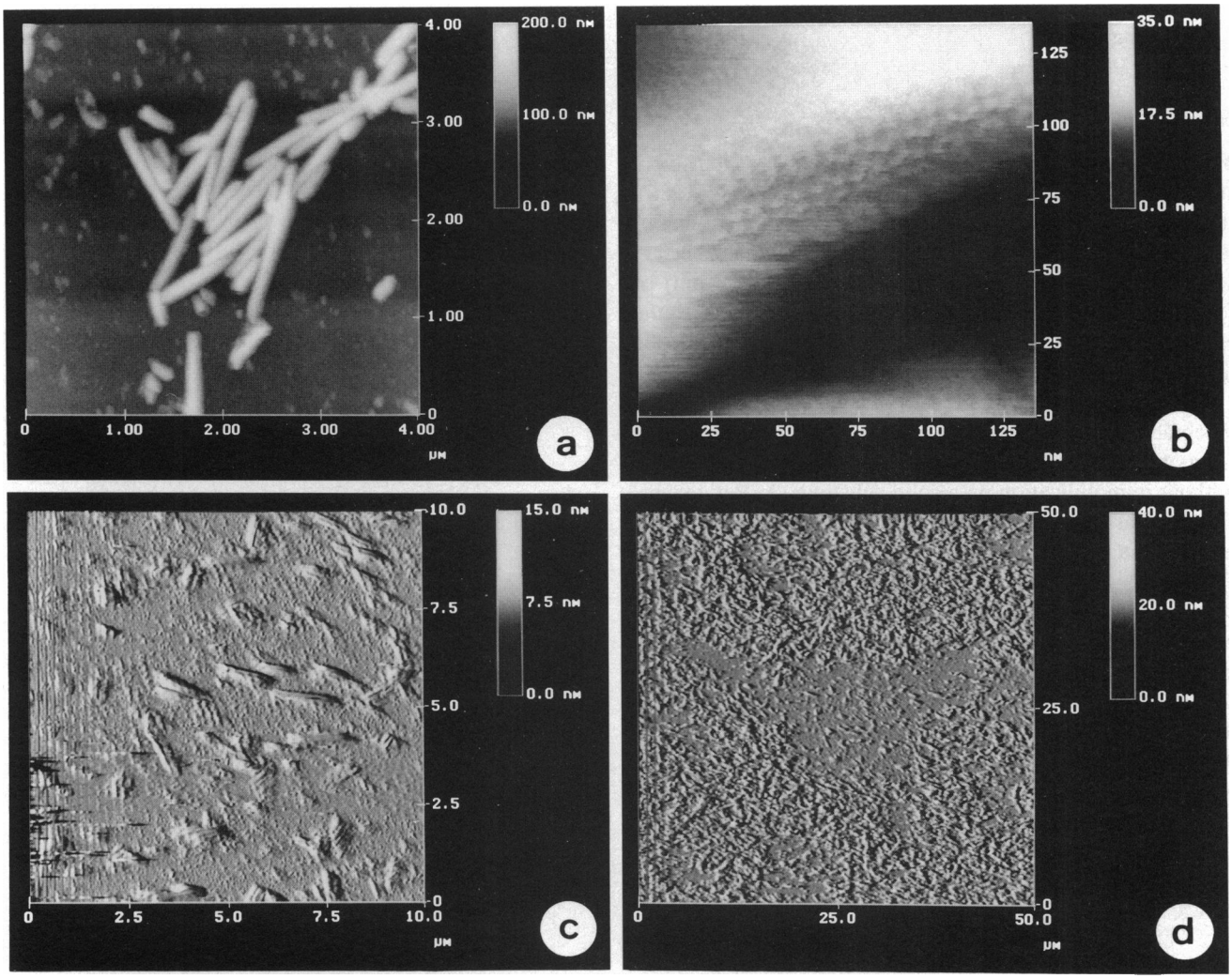

FIGURE 5 SFM images of bacteriophage T4 polyheads on derivatized glass in buffer solution. Distribution of polyheads (*a*) and capsomeres at higher magnification (*b*). The smaller features in the background of *a* are due to phage or polyhead fragments remaining in the solution during preparation and purification of the polyheads. Controls with preirradiated cross-linkers show that (*c*) no stable image can be obtained and (*d*) that the polyheads are wiped off over the whole scan area.

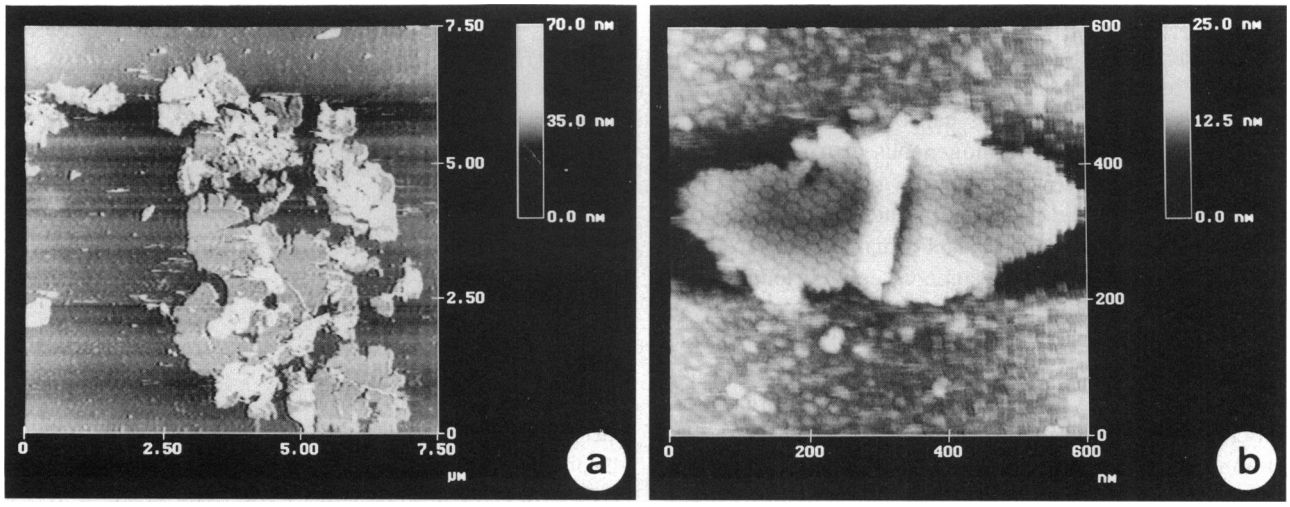

FIGURE 6 SFM images of the HPI layer on derivatized glass in buffer solution. The distribution of the layers is shown in *a*, while the hexagonal arrangement of doughnut-shaped units is discernible at higher magnification (*b*).

these conditions it was not possible to acquire any high resolution topographs.

HPI layer

The HPI layer of *D. radiodurans* has been extensively studied by electron microscopy (Baumeister et al., 1986). Its stability is remarkable: even after drying in air it exhibits a relatively well preserved structure (Wildhaber et al., 1985) showing a hexagonal lattice ($a = b = 18$ nm) of rosette-like units connected by six spokes. Therefore, the HPI layer has been used as a test object for scanning probe microscopy at ambient pressure (Guckenberger et al., 1989; Stemmer and Engel, 1990; Wang et al., 1990; Wiegräbe et al., 1991; Schabert et al., 1992). Imaging HPI layers by the SFM in buffer solution has not been possible without immobilization on a solid substrate. At low magnification flat single layers are readily visible (Fig. 6 *a*). At higher magnification the hexagonal arrangement of doughnut-shaped units becomes apparent (Fig. 6 *b*). Instabilities of the *z* signal are correlated with multiple layers, whereas single and flat HPI layers could be imaged repeatedly at magnifications > 200,000 times. This is demonstrated in Fig. 7, where the difference between first (Fig. 7 *a*), third (Fig. 7 *b*), and sixth (Fig. 7 *c*) scan is hardly visible. As indicated by the diffraction patterns (*insets*), structural details are preserved to at least 1.6 nm, and the resolution appears to improve during repetitive scans. The thickness of single HPI layers was 6.6 ± 0.5 nm ($n = 18$), whereas stable double layers exhibited a thickness of 17.2 ± 1.4 nm ($n = 15$).

Reconstituted intermediate filaments

Intermediate filaments are essential cytoskeletal constituents of differentiated eukaryotic cells (Stewart, 1990). To characterize the assembly process, cloned intermediate filament proteins have been modified by site-directed mutagenesis (Heitlinger et al., 1991). The wild-type neurofilament peptide NF-L expressed in *E. coli* has been reconstituted to 10-nm filaments, and their shape, length and width have been determined by electron microscopy (Heins et al., 1993). As illustrated here, their thickness can be measured with the SFM. Fig. 8 *a* shows the homogeneous distribution of the filaments immobilized on the modified glass surface. Higher magnification scans did not unveil structural details in this experiment, although the filaments remained stable during scanning (Fig. 8, *b* and *c*). In some cases their tendency to unravel into protofilaments could clearly be seen (Fig. 8 *d*). The measured height (9.5 ± 1.2 nm, $n = 100$) is comparable to the width (10.4 ± 1.0 nm, $n = 100$) from electron microscopy (Heins et al., 1993), suggesting a cylindrical filament cross-section. While the observed filament length distribution was identical to that seen in the electron microscope, the widths obtained from the SFM were larger by a factor of 5 compared to those measured with the electron microscope.

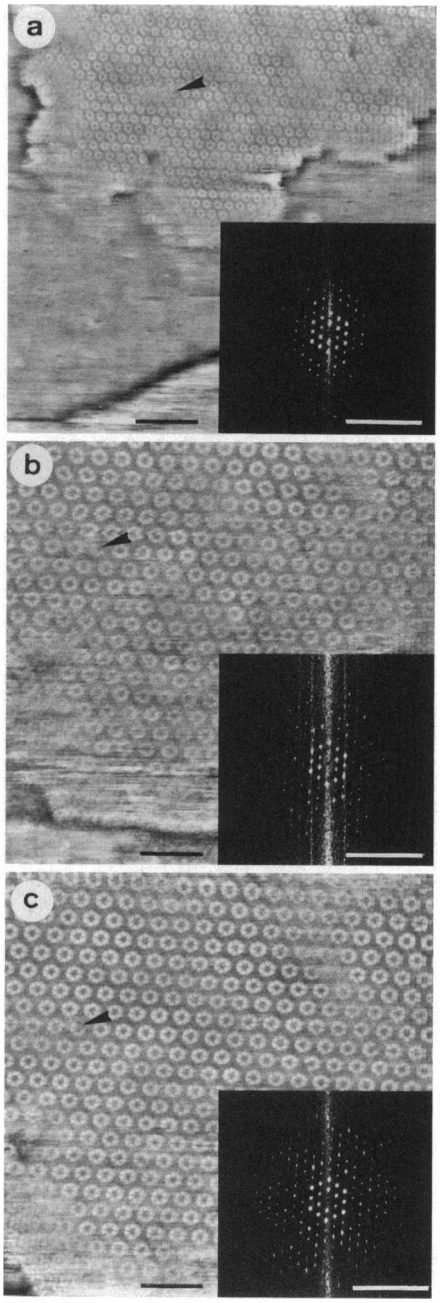

FIGURE 7 Image reproducibility. The area displayed in *a* has been scanned at higher magnification several times. *b* shows the third and *c* the sixth scan. The arrowheads point to a small defect that is seen in every scan. In all images the linear gradient and frequency components below $(19\ \text{nm})^{-1}$ were removed. Diffraction patterns (*insets*) were calculated after flattening from identical areas comprising 135 HPI unit cells. Scale bars are 100 nm in *a*, 50 nm in *b* and *c*, and $(2\ \text{nm})^{-1}$ in all insets.

TMV

Tobacco mosaic virus is often used as a test specimen as its atomic structure is available (Namba and Stubbs, 1986). It has been studied by conventional transmission electron microscopy (Unwin and Klug, 1974; Jeng et al., 1989) and scanning tunneling microscopy (Stemmer et al., 1989). Although the 2.3-nm periodicity of the virus structure could be

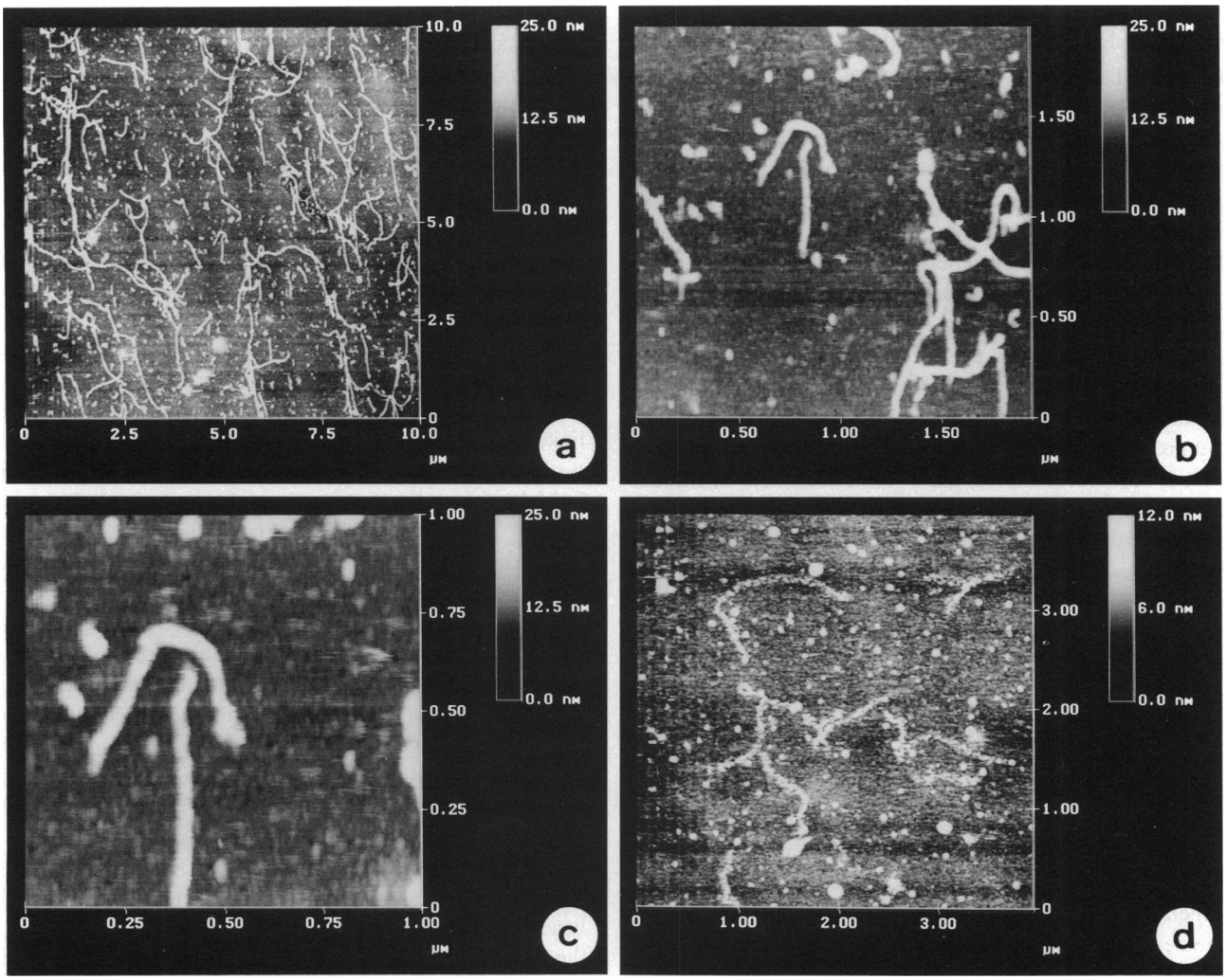

FIGURE 8 SFM images of intermediate filaments on derivatized glass in buffer solution. (*a*) Distribution of the filaments. The smaller features in the background represent either tetramers of the NF-L polypeptide or polymerization products from the chemical modification. (*b* and *c*) No structural details can be seen at higher magnification, but the filaments remain stable during scanning. (*d*) In some cases unravelling of the intermediate filaments into protofilaments is visible.

seen in the scanning tunneling microscope (Stemmer et al., 1989), it was not possible to obtain images of comparable quality with the SFM. Our best images were from TMV particles adsorbed to polylysine-coated coverslips in isopropanol. The width of well preserved rods was 67.6 ± 12.4 nm ($n = 30$) and their height was 14.9 ± 3.4 nm ($n = 30$). Such samples were not sufficiently stable to allow high magnification scans. Moreover, for as yet unknown reasons, the polylysine coat had rather variable properties. No high quality images could be collected using the cross-linker method, even when the glass plates were clamped at 5×10^3 N/cm^2 to ensure a close contact of the hydrophilic TMV particles to the hydrophobic glass surface. Rod-like structures of appropriate dimensions could be discerned (data not shown), but they were sparse and frequently led to pronounced instabilities of the z signal. Parallel experiments with Pt/C-coated air-dried TMV preparations inspected by SEM showed that the rods were evenly and densely distributed on the glass surfaces.

DISCUSSION

Scanning force microscopy opens new avenues for gathering structural data from a biological surface that are complementary to data collected by other microscopical techniques. While imaging biological structures with the SFM in air is limited by drying artifacts (Kellenberger and Kistler, 1979) and capillary forces (Weisenhorn et al., 1989), major progress is expected from the possibility to image samples in buffer solution (Drake et al., 1989). Propanol was used instead of aqueous solution mainly with nucleic acids and DNA-protein complexes (Hansma et al., 1992; Vesenka et al., 1992b; Lyubchenko et al., 1993; Shaiu et al., 1993). However, it should be noted that ethanol dehydration of DNA adsorbed to an uncharged carbon film yields fibers that appear either beaded or with knob-like protrusions along their axis (Eickbush and Moudrianakis, 1978). Biomacromolecules that are weakly adsorbed to a solid support can easily be displaced during scanning. Thus far, reproducible

imaging in buffer at a lateral resolution between 1.1 and 2.5 nm has only been demonstrated with purple membranes (Butt et al., 1990) and gap junctions (Hoh et al., 1993) as well as membrane-bound Fab fragments (Weisenhorn et al., 1990) and cholera toxin (Yang et al., 1993). While these large planar and polar structures interact strongly with the negatively charged surface of freshly cleaved mica in the presence of divalent cations, new methods for immobilizing filaments and single biomacromolecules are required.

Here we present a protocol that is simple, does not require any special equipment, and is suited to covalently bind biological samples to glass or silicon surfaces. Glass surfaces have been reported to be rough compared to mica or silicon wafers that are often used as specimen substrates for scanning probe microscopy (Goettgens et al., 1992; Radmacher et al., 1993). Nevertheless, glass surfaces that are as smooth as silicon wafers can be obtained with the washing procedures described above (Table 1, Fig. 4 *b*). In any case, the chemical modification introduces surface corrugations that are not negligible. Compared to silicon wafers or mica, which both can be chemically activated (Lyubchenko et al., 1993), the major advantage of coverslips is that they are transparent and of excellent optical quality and therefore suitable for combining SFM and light microscopy (Schabert et al., 1993).

Many different protocols for silanizing surfaces have been described (Robinson et al., 1971; Weetall, 1976; Machleidt and Wachter, 1977; Aebersold et al., 1986; Wassermann et al., 1989; Vandenberg et al., 1991b; Kurth and Bein, 1992). The reaction conditions used, i.e., deposition method, time, temperature, curing, and solvents varied considerably. To silanize coverslips with APTES, we have followed the method of Aebersold et al. (1986). In our hands, this method yielded an average packing density of 6 NH_2 groups/nm^2 of glass surface, a value similar to that reported for films adsorbed from vapor (Kurth and Bein, 1992). In spite of a short reaction time (3 min) the increase of the surface roughness after silanization may suggest APTES polymerization characteristic for solution deposition (Vandenberg et al., 1991a). We have selected this protocol because it is simple and involves mild conditions under which silanization occurs. As outlined by Vandenberg et al. (1991a), mild conditions are preferred when coverage of surfaces with a monolayer of functional groups is intended.

The most important aspect of a silanization reaction is the orientation of the APTES molecules on the support, as this influences surface properties and subsequent chemical reactions: efficient coupling of the cross-linker can only take place if the free amino groups are accessible. Although we have confirmed their presence by the ninhydrin reaction, the high hydrophobicity of the silanized surface (Table 2) could indicate that only a small fraction of the amino groups is actually exposed. Amino groups facing the glass surface represent APTES molecules bound by electrostatic interactions; thus, such molecules should be removed by alkaline treatment. However, even incubation for 4 h at pH 10 did not significantly change the hydrophobicity of the glass surface (Table 2). Therefore, we conclude that most aminopropyl groups are linked by covalent bonds to the glass surface.

To immobilize samples to derivatized glass surfaces, we have selected the photoactivatable heterobifunctional cross-linker ANB-NOS. As a succinimide ester it reacts with NH_2 groups to form an amide bond. After photoactivation, the azido group is converted to a highly reactive nitrene, which can undergo a variety of insertion and addition reactions (Reiser and Wagner, 1971). Considering the diversity of biological structures one may wish to immobilize for examination in the SFM, this property of ANB-NOS and other azido cross-linkers is advantageous. ANB-NOS was selected for two reasons. First, the relatively high yield of coupling determined with AP as compared to other cross-linkers we have tested, i.e., sulfosuccinimidyl 2-(*m*-azido-*o*-nitrobenzamido)-ethyl-1,3′-dithiopropionate, disuccinimidyl tartrate, disulfosuccinimidyl tartrate, bis(sulfosuccinimidyl) suberate, *p*-azidophenylisothiocyanate. Second, irradiation damage of proteins is negligible at the peak wavelength of photolysis (320–350 nm). As illustrated in Fig. 1, UV irradiation at 366 nm suffices to activate the photosensitive group. As revealed by visual comparison of the topographs shown in Fig. 4, the chemical modifications introduce a certain surface roughness that is also reflected by the root-mean-square values of the *z* values from such images (Table 1). These corrugations may cause problems when small biomacromolecules are to be imaged, as these are probably difficult to discriminate against the background.

We have used test objects that have been studied extensively by electron microscopy, i.e., bacteriophage T4 polyheads, the HPI layer, intermediate filaments, and TMV. With the exception of TMV, all of these structures could be immobilized efficiently to the glass surfaces. This indicates that covalent binding depends critically on the properties of the protein structure studied. A compact and rigid structure such as the hydrophilic TMV rod, for example, does not react with the rather hydrophobic cross-linker. Even when pressed onto the glass surface at 5×10^3 N/cm^2 during photoactivation, TMV particles were not sufficiently bound that they could withstand imaging with the SFM at high magnification. Other structures, such as the polyheads or the intermediate filaments, possess a more open and flexible surface, which is accessible to the photoactivatable cross-linker. Therefore, the nitrene can readily react with these proteins and immobilize them. The extracellular surface of the HPI layer could reproducibly be imaged at high resolution (Fig. 7), whereas images of the inner surface were not found. Thus, the inner HPI layer surface appears to adsorb predominantly to the modified glass surface and is efficiently bound to it by UV-activated ANB-NOS. This is explained by hydrophobic interactions that promote the tight association of the HPI layer with the outer membrane of *D. radiodurans* in vivo (Baumeister et al., 1986).

The native preservation of the HPI layer is evidenced by height measurements: hydrated single layers have a thickness of 6.6 ± 0.5 nm (n = 18) and double layers 17.2 ± 1.4 nm (n = 15). These values are in close agreement with electron

microscopy data of freeze-dried unstained HPI layers recorded by scanning transmission electron microscopy (6.9 ± 0.3 nm; Engel et al., 1982) and freeze-fractured HPI layer stacks (7.7 ± 1.0 nm; Wildhaber et al., 1985). Much smaller values that depend significantly on the substrate have been reported for metal coated HPI layers (Guckenberger et al., 1989). The high values for double layers, as compared to single layers, may be explained by carbohydrates that interact with the adjacent layer (Baumeister et al., 1986). A further indication of the excellent structural preservation is provided by the diffraction pattern of Fig. 7 *c* that suggests a lateral resolution of 1.6 nm. There is a compelling correlation between the fine structure of the HPI layer as seen by the SFM and by electron microscopy that is currently analyzed (Karrasch et al., 1993). The interactions between protein structures and the modified glass surface are weak enough to allow polyheads to retain their cylindrical shape: their height measured by the SFM is 57 ± 13.8 nm, which is in good agreement with their diameter of 50–65 nm (Steven et al., 1976). In addition, the upper side of the tubes does not have any contact with the chemically modified glass surface and is therefore in its native state.

When imaging filamentous molecules like the intermediate filaments or cylindrical structures like TMV and polyheads with the SFM, the influence of the tip geometry becomes evident. Height measurements from the SFM are consistent with width measurements from electron microscopy, whereas the widths determined with the SFM are too large. From the apparent width W and height $2r$ of an image from a cylindrical structure the tip radius R can be estimated (Keller and Chin-Chung, 1992; Vesenka et al., 1992a; Zenhausern et al., 1992) according to $W = 4(Rr)^{1/2}$. In the case of intermediate filaments (W = 52 nm, $2r$ = 10.4 nm), this equation yields a tip radius R = 32 nm.

CONCLUSION

Here we present a reproducible method for binding proteins covalently to chemically modified glass surfaces. Different protein structures immobilized by our protocol were imaged at high resolution in buffer solution with the SFM. The limitations of the method are related to the surface properties of the modified coverslips that hinder efficient binding of hydrophilic and rigid protein structures. Further developments should aim at a reduction of the surface roughness and hydrophobicity.

We thank Drs. U. Aebi and J. H. Hoh for critical discussions, and Drs. W. Baumeister, J. Witz, and S. Heins for providing samples. This work was supported by the Swiss National Foundation for Scientific Research, grant 31-32536.91 (to A. E.), the Research Foundations of Ciba-Geigy, Hoffmann-La Roche and Sandoz, and the M. E. Müller-Foundation of Switzerland.

REFERENCES

Aebersold, R. H., D. B. Teplow, L. E. Hood, and S. B. H. Kent. 1986. Electroblotting onto activated glass. *J. Biol. Chem.* 261:4229–4238.

Albrecht, T. R., S. Akamine, T. E. Carver, and C. F. Quate. 1990. Microfabrication of cantilever styli for the atomic force microscope. *J. Vac. Sci. Technol. A.* 8:3386–3396.

Albrecht, T. R., and C. F. Quate. 1987. Atomic resolution imaging of a nonconductor by atomic force microscopy. *J. Appl. Phys.* 62:2599–2602.

Alves, C. A., E. L. Smith, and M. D. Porter. 1992. Atomic-scale imaging of alkanethiolate monolayers at gold surfaces with atomic force microscopy. *J. Am. Chem. Soc.* 114:1222–1227.

Anderson, G. W., J. E. Zimmermann, and F. M. Callahan. 1964. The use of esters of N-hydroxysuccinimide in peptide synthesis. *J. Am. Chem. Soc.* 86:1839–1842.

Aplin, J. D., R. C. Hughes, C. L. Jaffe, and N. Sharon. 1981. Reversible cross-linking of cellular components of adherent fibroblasts to fibronectin and lectin-coated substrata. *Exp. Cell Res.* 134:488–494.

Baumeister, W., M. Barth, R. Hegerl, R. Guckenberger, M. Hahn, and W. O. Saxton. 1986. Three-dimensional structure of the regular surface layer (HPI layer) of *Deinococcus radiodurans*. *J. Mol. Biol.* 187:241–253.

Binnig, G., C. F. Quate, and C. Gerber. 1986. Atomic force microscope. *Phys. Rev. Lett.* 56:930–933.

Binnig, G., C. Gerber, E. Stoll, T. R. Albrecht, and C. F. Quate. 1987. Atomic resolution with atomic force microscopy. *Europhys. Lett.* 3: 1281–1286.

Brode, P. F., and D. S. Rauch. 1992. Subtilisin BPN′: activity on an immobilized substrate. *Langmuir.* 8:1325–1329.

Butt, H-J., K. H. Downing, and P. K. Hansma. 1990. Imaging the membrane protein bacteriorhodopsin with the atomic force microscope. *Biophys. J.* 58:1473–1480.

Decker, L. A., editor. Worthington Enzyme Manual. 1977. Worthington Biochemical Corporation: Freehold, NJ.

Drake, B., C. B. Prater, A. L. Weisenhorn, S. A. C. Gould, T. R. Albrecht, C. F. Quate, D. S. Cannell, H. G. Hansma, and P. K. Hansma. 1989. Imaging crystals, polymers, and processes in water with the atomic force microscope. *Science (Wash. DC).* 243:1586–1589.

Eickbush, T. H., and E. N. Moudrianakis. 1978. The compaction of DNA helices into either continuous supercoils or folded-fiber rods and toroids. *Cell.* 13:295–306.

Engel, A., W. Baumeister, and W. O. Saxton. 1982. Mass mapping of a protein complex with the scanning transmission electron microscope. *Proc. Natl. Acad. Sci. USA.* 79:4050–4054.

Engel, A., A. Hoenger, A. Hefti, C. Henn, R. Ford, C. J. Kistler, and M. Zulauf. 1992. Assembly of 2-D membrane protein crystals: dynamics, crystal order, and fidelity of structure analysis by electron microscopy. *J. Struct. Biol.* 109:219–234.

Goettgens, B. M., R. W. Tillmann, M. Radmacher, and H. E. Gaub. 1992. Molecular order in polymerizable Langmuir-Blodgett films probed by microfluorescence and scanning force microscopy. *Langmuir.* 8: 1768–1774.

Guckenberger, R., W. Wiegräbe, A. Hillebrand, T. Hartmann, Z. Wang, and W. Baumeister. 1989. Scanning tunneling microscopy of a hydrated bacterial surface protein. *Ultramicroscopy.* 31:327–332.

Hansma, G. H., J. Vesenka, C. Siegerist, G. Keldermann, H. Morrett, R. L. Sinsheimer, V. Elings, C. Bustamante, and P. K. Hansma. 1992. Reproducible imaging and dissection of plasmid DNA under liquid with the atomic force microscope. *Science (Wash. DC).* 256:1180–1184.

Heins, S., P. C. Wong, S. Müller, K. Goldie, D. W. Cleveland, and U. Aebi. 1993. The rod domain of NF-L determines neurofilament architecture, whereas the end domains specify filament assembly and network formation. *J. Cell Biol.* In press.

Heitlinger, E., M. Peter, M. Häner, A. Lustig, U. Aebi, and E. A. Nigg. 1991. Expression of chicken lamin B_2 in *Escherichia coli*: characterization of its structure, assembly, and molecular interactions. *J. Cell Biol.* 113: 485–495.

Hendry, R. M., and D. S. Rauch. 1980. Immobilization of antibodies on nylon for use in enzyme-linked immunoassay. *J. Immunol. Methods.* 35: 285–296.

Hillner, P. E., A. J. Gratz, S. Manne, and P. K. Hansma. 1992. Atomic-scale imaging of calcite growth and dissolution in real time. *Geology.* 20: 359–362.

Hoh, J. H., G. E. Sosinsky, J.-P. Revel, and P. K. Hansma. 1993. Structure of the extracellular surface of the gap junction by atomic force microscopy. *Biophys. J.* 65:149–163.

Jacobson, B. S., and D. Branton. 1977. Plasma membrane: rapid isolation and exposure of the cytoplasmic surface by use of positively charged beads. *Science (Wash. DC)*. 195:302–304.

Jeng, T-W., R. A. Crowther, G. Stubbs, and W. Chin. 1989. Visualization of alpha-helices in tobacco mosaic virus by cryo-electron microscopy. *J. Mol. Biol.* 205:251–257.

Karrasch, S., R. Hegerl, J. H. Hoh, W. Baumeister, and A. Engel. 1993. Atomic force microscopy produces faithful high resolution images of protein surfaces in an aqueous environment. *Proc. Natl. Acad. Sci. USA*. In press.

Kellenberger, E., and J. Kistler. The physics of specimen preparation. *In* Unconventional Electron Microscopy for Molecular Structure Determination. W. R. Hoppe Mason, editor. 1979. Vieweg, Braunschweig, Germany. 49–79.

Keller, D., and C. Chin-Chung. 1992. Imaging steep, high structures by scanning force microscopy with electron beam deposited tips. *Surf. Sci.* 268:333–339.

Kurth, D. G., and T. Bein. 1992. Monomolecular layers and thin films of silane coupling agents by vapor-phase adsorption on oxidized aluminium. *J. Phys. Chem.* 96:6707–6712.

Lewis, R. V., M. F. Roberts, E. A. Dennis, and W. S. Allison. 1977. Photoactivated heterobifunctional cross-linking reagents which demonstrate the aggregation state of phospholipase A_2. *Biochemistry*. 16:5650–5654.

Lyubchenko, Y. L., P. I. Oden, D. Lampner, S. M. Lindsay, and K. A. Dunker. 1993. Atomic force microscopy of DNA and bacteriophage in air, water and propanol: the role of adhesion forces. *Nucleic Acids Res.* 21:1117–1123.

Machleidt, W., and E. Wachter. 1977. New supports in solid-phase sequencing. *Methods Enzymol.* 47:263–277.

Manne, S., P. K. Hansma, J. Massie, V. B. Elings, and A. A. Gewirth. 1991. Atomic-resolution electrochemistry with the atomic force microscope: copper deposition on gold. *Science (Wash. DC)*. 251:183–186.

Namba, K., and G. Stubbs. 1986. Structure of tobacco mosaic virus at 3:6 A resolution: implications for assembly. *Science (Wash. DC)*. 231: 1401–1406.

Quash, G., A-M. Roch, A. Niveleau, J. Grange, T. Keolouangkhot, and J. Huppert. 1978. The preparation of latex particles with covalently bound polyamines, Ig G and measles agglutinins and their use in visual agglutination tests. *J. Immunol. Methods*. 22:165–174.

Radmacher, M., R. W. Tillmann, and H. E. Gaub. 1993. Imaging viscoelasticity by force modulation with the atomic force microscope. *Biophys. J.* 64:735–742.

Reiser, A., and H. M. Wagner. 1971. The photochemistry of the azido group. *In* The Chemistry of the Azido Group. S. Patai, editor. Interscience Publishers, New York.

Robinson, P. J., P. Dunnill, and M. D. Lilly. 1971. Porous glass as a solid support for immobilization or affinity chromatographie of enzymes. *Biochim. Biophys. Acta*. 242:659–661.

Sarin, V. K., S. B. H. Kent, J. P. Tamm, and R. B. Merrifield. 1981. Quantitative monitoring of solid-phase peptide synthesis by the ninhydrin reaction. *Anal. Biochem.* 117:147–157.

Saxton, W. O., T. J. Pitt, and M. Horner. 1979. Digital image processing: the Semper system. *Ultramicroscopy*. 4:343–354.

Schabert, F., A. Hefti, K. Goldie, A. Stemmer, and A. Engel. 1992. Ambient-pressure scanning probe microscopy of 2D regular protein arrays. *Ultramicroscopy*. 42:44:1118–1124.

Schabert, F., H. F. Knapp, S. Karrasch, R. Häring, and A. Engel. 1993. A confocal scanning laser—scanning probe hybrid microscope for biological applications. *Ultramicroscopy*. In press.

Shaiu, W-L., D. D. Larson, J. Vesenka, and E. Henderson. 1993. Atomic force microscopy of oriented linear DNA molecules labeled with 5 nm gold spheres. *Nucleic Acids Res.* 21:99–103.

Smith, R. J., R. A. Capaldi, D. Muchmore, and F. Dahlquist. 1978. Cross-linking of ubiquinone cytochrome *c* reductase (complex III) with periodate-cleavable bifunctional reagents. *Biochemistry*. 17:3719–3723.

Stemmer, A., and A. Engel. 1990. Imaging biological macromolecules by STM: quantitative interpretation of topographs. *Ultramicroscopy*. 34:129–140.

Stemmer, A., A. Hefti, U. Aebi, and A. Engel. 1989. Scanning tunneling and transmission electron microscopy on identical areas of biological specimens. *Ultramicroscopy*. 30:263–280.

Steven, A. C., E. Couture, U. Aebi, and M. K. Showe. 1976. Structure of T4 polyheads. *J. Mol. Biol.* 106:187–221.

Stewart, M. 1990. Intermediate filaments: structure, assembly and molecular interactions. *Curr. Opin. Cell Biol.* 2:91–100.

Unwin, P. N. T., and A. Klug. 1974. Electron microscopy of the aggregate of tobacco mosaic virus protein. I. Three-dimensional image reconstruction. *J. Mol. Biol.* 87:641–656.

Vandenberg, E. T., L. Bertilsson, B. Liedberg, K. Uvdal, R. Erlandsson, H. Elwing, and I. Lundström. 1991a. Structure of 3-aminopropyl triethoxy silane on silicon oxide. *J. Coll. Interface Sci.* 147:103–118.

Vandenberg, E. T., H. Elwing, A. Askendal, and I. Lundström. 1991b. Protein immobilization to 3-aminopropyl triethoxy silane/glutaraldehyde surfaces: characterization by detergent washing. *J. Coll. Interface Sci.* 143:327–335.

Vesenka, J., M. Guthold, C. L. Tang, D. Keller, E. Delaine, and C. Bustamante. 1992a. Substrate preparation for reliable imaging of DNA molecules with the scanning force microscope. *Ultramicroscopy*. 42:44: 1243–1249.

Vesenka, J., H. Hansma, C. Siegerist, G. Siligardi, E. Schabtach, and C. Bustamante. 1992b. Scanning force microscopy of circular DNA and chromatin in air and propanol. *SPIE*. 1639:127–137.

Wachter, E., W. Machleidt, H. Hofner, and J. Otto. 1973. Aminopropyl glass and its p-phenylene diisothiocyanate derivative, a new support in solid-phase Edman degradation of peptides and proteins. *FEBS Lett.* 35: 97–102.

Wang, Z., T. Hartmann, W. Baumeister, and R. Guckenberger. 1990. Thickness determination of biological samples with a z-calibrated scanning tunneling microscope. *Proc. Natl. Acad. Sci. USA*. 87:9343–9347.

Wassermann, S. R., Y-T. Tao, and G. M. Whitesides. 1989. Structure and reactivity of alkylsiloxane monolayers formed by reaction of alkyltrichlorosilanes on silicon subtrates. *Langmuir*. 5:1074–1087.

Weetall, H. H. 1976. Covalent coupling methods for inorganic support materials. *Methods Enzymol.* 44:134–148.

Weisenhorn, A. L., P. K. Hansma, T. R. Albrecht, and C. F. Quate. 1989. Forces in atomic force microscopy in air and water. *Appl. Phys. Lett.* 54:2651–2653.

Weisenhorn, A. L., B. Drake, C. B. Prater, S. A. C. Gould, P. K. Hansma, F. Ohnesorge, M. Egger, S-P. Heyn, and H. E. Gaub. 1990. Immobilized proteins in buffer imaged at molecular resolution by atomic force microscopy. *Biophys. J.* 58:1251–1258.

Wiegräbe, W., M. Nonnenmacher, R. Guckenberger, and O. Wolter. 1991. Atomic force microscopy of a hydrated bacterial surface protein. *J. Microsc.* 163:79–84.

Wildhaber, I., H. Gross, A. Engel, and W. Baumeister. 1985. The effects of air-drying and freeze-drying on the structure of a regular protein layer. *Ultramicroscopy*. 16:411–422.

Yang, J., L. K. Tamm, T. W. Tillack, and Z. Shao. 1993. New approach for atomic force microscopy of membrane proteins: The imaging of cholera toxin. *J. Mol. Biol.* 229:286–290.

Zenhausern, F., M. Adrian, B. ten Heggeler-Bordier, R. Emch, M. Jobin, M. Taborelli, and P. Descouts. 1992. Imaging of DNA by scanning force microscopy. *J. Struct. Biol.* 108:69–73.